Adaptive speed control of ROVs with experimental results from an aquaculture net pen inspection operation

Sveinung Johan Ohrem[1,†], Linn Danielsen Evjemo[1], Bent Oddvar Arnesen Haugaløkken[1], Herman Biørn Amundsen[1,2], Eleni Kelasidi[1]

***Abstract*— Remotely operated vehicles (ROVs) are often used for inspection in aquaculture net pens which serves the important purpose of localizing holes in the net and reporting potential irregularities and damages. Manual control of the vehicle inside a net pen, while simultaneously inspecting the net structure, is difficult and puts a lot of stress on the vehicle operators. Adaptation of new solutions that enables autonomous traversal of net pens where the vehicle maintains a fixed distance, heading, and velocity relative to the net is considered essential. One of the main challenges of such autonomous solutions is a robust and tight control of the vehicle's velocities. To target this challenge, this paper presents adaptive speed controllers for the surge and sway speeds of a remotely operated vehicle with unknown parameters and under the influence of unknown external disturbances. The stability properties of the controllers are proven through Lyapunov theory, and both simulations and field experiments demonstrate their ability to track the desired speeds through the use of a net following scheme.**

I. Introduction

Sea-based aquaculture is an industry facing several challenges related to inspection and maintenance of underwater structures such as net pens and mooring lines. Underwater cameras are often present inside the net pens for feed dispersion and fish behaviour monitoring, but these cameras are either static or can only move up and down and rotate. They are often located in the middle of the net pen, thus offering little information about the state of the net. Therefore, it is essential to adapt alternative solutions for precise inspection and monitoring of structures in fish farms, which is important if the industry is to improve on the Precision Fish Farming concept [1].

According to a recent study [2], the main cause of fish escapes is holes in the net. The holes are often caused by wear from the weight system, the main components of the net pen structure (e.g., mooring system, cage collar, and bottom ring chain), and external factors such as propellers on boats performing operations close to the net pen. The same study also shows that weather, environmental conditions, and operations in and around the fish cages are the most common circumstances in which fish escape from net pens [2]. Note that sea-based fish farms in Norway are exposed to significant environmental forces from winds, waves, and currents, and operations such as delousing, moving, and counting fish, at the fish farm, are quite common. Thus, it is essential to have better control of escaped farmed salmon, which also cause a threat to the wild salmon population through interbreeding and the spread of disease and sea lice [3], [4]. A recent regulation passed by the Norwegian government introduced requirements on fish farm proprietors to ensure necessary surveillance and monitoring before, during, and after any operation that may lead to fish escapes [5, §37.a].

Since the cameras used for feed and fish monitoring offer limited information about the nets, ROVs are commonly employed to inspect the net structures. Divers are also used for inspection of nets and structures in Norwegian aquaculture. Diving operations are heavily regulated and involve high risk. As fish farms continue to expand into more exposed locations, the use of divers for inspections may become challenging. However, a study suggests that while ROVs may not fully replace divers for all operations, they can significantly improve the risk and efficiency of inspection operations in aquaculture [6]. This highlights the value of incorporating ROVs into fish farm inspection strategies, particularly in more challenging environments.

The ROVs are mainly manually operated and the automatic functions are often limited to automatic depth and heading control. Automatic depth control is useful, but since the ROV is operating inside a cylindrical net pen, the automatic heading control function offers limited assistance to an operator as the desired heading angle often changes. Furthermore, the operator needs to both control the ROV and monitor the net structure simultaneously, which can be particularly challenging when the ROV is influenced by, e.g., ocean currents. The Norwegian Directorate of Fisheries reports several cases where holes in the net have not been detected by operators during inspections [7]. The operator must also maneuver the ROV with great care and make sure it does not crash into the net structure and potentially cause tears and holes. The aforementioned challenges alongside the fact that some industrial actors are moving their production to more exposed areas, which increases risk and reduces availability for humans, speak towards a need for more autonomous functionality in robotic operations in aquaculture [8].

Recent efforts have been made to increase the level of autonomy of ROVs operating in net pens. In particular, the work of [9] introduces a net-following algorithm utilizing a Doppler velocity logger (DVL) to measure the net-relative distance, heading, and velocity of the ROV, and employs the line-of-sight (LOS) guidance law [10] to enable auto-

*This work was supported by SINTEF Ocean, department of Aquaculture.

[1]Aquaculture robotics and automation, Department of Aquaculture, SINTEF Ocean AS, Trondheim, Norway.

[2]Department of Engineering Cybernetics, Norwegian University of Science and Technology, Trondheim, Norway.

†Corresponding author: sveinung.ohrem@sintef.no

matic horizontal traversal of the net structure at a fixed distance from the net. Results from field trials successfully demonstrate the net-following algorithm. In [11] the net-following algorithm of [9] is integrated in a mission control system that opens the possibilities for more advanced net inspection patterns. Again, the system is demonstrated in a field trial showing promising results. An alternative to DVLs for measuring the net-relative distance and heading is presented in [12]. Here, a system comprised of two lasers and the camera onboard the ROV are utilized. The results are comparable to those achieved with the DVL at a fraction of the price, but the system does not measure the net-relative velocity and it has yet to be tested in real-time and in closed-loop with the ROV control system.

The net-following and LOS approach reported in [9] utilized PI controllers in the field trials to control the surge and sway speed of the ROV, which were reported to provide insufficient accuracy for surge and sway speed control. It is further argued that controllers addressing model uncertainty could improve performance. An adaptive control scheme for positioning and velocity control is presented in [13] and results from field trials demonstrate that the proposed solution is quite precise. The scheme, however, relies on measurements from an ultra-short baseline (USBL) positioning system and a camera-based motion capture system, which may be unavailable in an aquaculture setting. In [14] the surge, sway, and heave speeds of an ROV, as well as the position, are controlled using a multi-input-multi-output (MIMO) PID controller synthesized from a feedback linearizing term and where a nonlinear high-gain observer is adapted to provide estimates of the system states. The controller is demonstrated in field trials and accurate tracking of the desired speeds and the position are obtained. Feedback linearizing control for an ROV performing net-following was introduced in [9], but due to plant-model mismatch causing instabilities, the controller was not tested in field trials. Furthermore, [14] utilized a high-precision underwater positioning system that, due to its cost and requirements for installation, may be unavailable for many ROV service companies operating in an aquaculture setting.

To summarize, velocity control of ROVs in net pens using PID controllers has been reported to lack precision, and feedback linearizing controllers have been reported to be unstable due to uncertainties in the model parameters. Furthermore, positioning systems such as USBL or optics-based solutions may require additional hardware installations and increase both the complexity and cost of the system, which may not be suited in an aquaculture setting. To address these issues, this paper proposes a speed controller for the surge and sway speeds of ROVs. The controller utilizes an adaptive term and does not require knowledge of the system parameters. The presented controller is derived from a recently developed adaptive backstepping dynamic positioning (DP) controller [15]. Through Lyapunov analysis, it is shown that the proposed speed controller ensures that the error system and the parameter estimation system are stable and that the error system converges to zero. The proposed controller was validated in a simulation environment and in a field trial at an industrial-scale fish farm under realistic operating conditions.

The paper is structured as follows: Section II introduces the control plant model of an ROV used for deriving the control law. Section III considers the control design and the stability proof. Section IV presents the results from simulations and field trials while Section V concludes the paper.

II. ROV Model

The velocity of an ROV can be expressed as the velocity of a reference frame fixed on the ROV relative to an inertial reference frame. The ROV-fixed reference frame is often referred to as the BODY frame while the North-East-Down (NED) frame is often used as the inertial frame in marine system modelling [16]. For the model adapted in this paper, the following assumptions are introduced:

Assumption 1: The ROV is symmetric about the port-starboard, fore-aft, and bottom-top axes, has negligible roll and pitch angles and the center of gravity coincides with the center of buoyancy and the center of origin.

Assumption 2: The vehicle is neutrally buoyant.

Assumption 3: The vehicle operates at low speeds, as such the contributions from the Coriolis and centripetal forces are dominated by linear and nonlinear damping forces and are thus omitted from the model.

Remark 1: Assumptions 1-3 are common when modelling ROVs [17], [16].

Assumption 4: The ocean currents and 1st-order wave forces are considered constant and irrotational in the horizontal NED frame and are modelled as an external disturbance force.

Remark 2: Assumption 4 is widely adapted for modeling of ROVs [16]. Even though the ocean current flow field inside a net pen can be quite complex [18], the flow speed is lower than on the outside of the net pen. Modelling the ocean current as an external force obviates the need for the relative velocity vector which may require measurements of the ocean current [17, Ch. 2.4.3]. Assumption 4 might be somewhat strict for an aquaculture-related setting but is introduced for control plant modelling purposes. It is later demonstrated through experiments that the controller achieves the control objective regardless of this simplifying assumption.

Assumption 5: The parameters of the mass and damping matrices of the ROV are constant.

Remark 3: Assumption 5 is common in adaptive control [19], [16, Ch.13.2.5].

Assumption 6: The heading angle and the depth of the ROV converge to their respective desired values.

Remark 4: The work presented in this paper concerns speed control of the surge and sway degrees of freedom. As such, the heading and depth degrees of freedom are considered to be controlled by suitable controllers able to bring the heading and depth to their desired values. In this paper, a controller similar to that of [15] is used for heading

and depth control, however, any controller capable of driving the controlled state to the desired value could be used.

The dynamic model of the ROV [16], considering two degrees of freedom (i.e., surge and sway) is given as

$$\dot{\boldsymbol{\eta}} = \boldsymbol{R}(\psi)\boldsymbol{\nu} \tag{1}$$

$$\boldsymbol{M}\dot{\boldsymbol{\nu}} + \boldsymbol{D}_l\boldsymbol{\nu} + \boldsymbol{D}_n(\boldsymbol{\nu})\boldsymbol{\nu} = \boldsymbol{\tau} + \boldsymbol{\tau}_c^b \,. \tag{2}$$

Here, $\boldsymbol{\eta} = \begin{bmatrix} N & E \end{bmatrix}^{\mathrm{T}}$ describes the North and East position of the vehicle in the NED frame. $\boldsymbol{R}(\psi)$ is a rotation matrix between the BODY and NED frames, given as

$$\boldsymbol{R}(\psi) = \begin{bmatrix} \cos(\psi) & -\sin(\psi) \\ \sin(\psi) & \cos(\psi) \end{bmatrix} \tag{3}$$

and ψ is the heading angle of the vehicle. Further, $\boldsymbol{\nu} = \begin{bmatrix} u & v \end{bmatrix}^{\mathrm{T}}$ where u and v are the surge and sway speeds, respectively, $\boldsymbol{M} \in \mathbb{R}^{2\times 2}$ is the system inertia matrix with

$$\boldsymbol{M} = \mathrm{diag}\left[m - X_{\dot{u}},\, m - Y_{\dot{v}}\right] \tag{4}$$

where m is the mass of the vehicle and $X_{\dot{u}}$ and $Y_{\dot{v}}$ are the added mass terms in the surge and sway degree of freedom, respectively. Moreover, $D_l > 0 \in \mathbb{R}^{2\times 2}$ is the linear damping matrix and $D_n > 0 \in \mathbb{R}^{2\times 2}$ is the nonlinear damping matrix, i.e.,

$$\boldsymbol{D}_l = -\mathrm{diag}\left[X_u,\, Y_v\right] \tag{5}$$

$$\boldsymbol{D}_n(\boldsymbol{\nu}) = -\mathrm{diag}\left[X_{|u|u}|u|,\, Y_{|v|v}|v|\right] \,, \tag{6}$$

where X_u and Y_v are the linear damping terms and $X_{|u|u}$ and $Y_{|v|v}$ are the nonlinear damping terms.

The control input is given by $\boldsymbol{\tau} \in \mathbb{R}^2$ and the external disturbance from the ocean current and 1st order wave forces, in the BODY frame, is given by $\boldsymbol{\tau}_c^b = \begin{bmatrix} \tau_c^u & \tau_c^v \end{bmatrix}^{\mathrm{T}} \in \mathbb{R}^2$.

Remark 5: The current and wave disturbances in the BODY frame are non-constant because the vehicle is moving and rotating. The current and wave forces in the inertial NED frame (which are assumed constant) are projected to the BODY frame through

$$\boldsymbol{\tau}_c^b = \boldsymbol{R}^{\mathrm{T}}(\psi)\boldsymbol{\tau}_c \,, \tag{7}$$

where $\boldsymbol{\tau}_c = \begin{bmatrix} \tau_c^N & \tau_c^E \end{bmatrix}^{\mathrm{T}}$ are the current and wave forces in the NED frame.

III. Control design

In this section, the proposed speed control design and stability proof are presented.

The vector containing the desired speeds is defined as $\boldsymbol{\nu}_d = \begin{bmatrix} u_d & v_d \end{bmatrix}^{\mathrm{T}}$. This vector is generated by passing the reference speeds, i.e., u_r and v_r, through reference models [16, Ch.10.2] that generate smooth desired speed signals, u_d and v_d, and desired accelerations, $\dot{u}_d$ and $\dot{v}_d$. The reference models are of 2nd order and have the form

$$\ddot{u}_d + 2\zeta_u\omega_u\dot{u}_d + \omega_u^2 u_d = \omega_u^2 u_r \tag{8}$$

$$\ddot{v}_d + 2\zeta_v\omega_v\dot{v}_d + \omega_v^2 v_d = \omega_v^2 v_r \,, \tag{9}$$

where ζ_u, ζ_v are the damping ratios and ω_u, ω_v are the natural frequencies of the reference models.

The error variable is then defined as

$$\boldsymbol{e} = \boldsymbol{\nu} - \boldsymbol{\nu}_d \,, \tag{10}$$

which has time derivative

$$\begin{aligned} \dot{\boldsymbol{e}} &= \dot{\boldsymbol{\nu}} - \dot{\boldsymbol{\nu}}_{\boldsymbol{d}} \\ &= \boldsymbol{M}^{-1}\left(-\boldsymbol{D}_l\boldsymbol{\nu} - \boldsymbol{D}_n(\boldsymbol{\nu})\boldsymbol{\nu} + \boldsymbol{\tau} + \boldsymbol{R}^{\mathrm{T}}(\psi)\boldsymbol{\tau}_c\right) - \dot{\boldsymbol{\nu}}_{\boldsymbol{d}} \,, \end{aligned} \tag{11}$$

where (2) and (7) have been applied.

The parameters of the mass and damping matrices of (11) are unknown and, thus, to handle these uncertainties and the uncertainties introduced by external disturbances an adaptive control approach is suggested in the following Theorem.

Theorem 1: Considering the plant model in (1)-(2) under Assumptions 1-5, the controller

$$\boldsymbol{\tau} = -\boldsymbol{K}\boldsymbol{e} + \boldsymbol{\phi}\left(\dot{\boldsymbol{\nu}}_d, \boldsymbol{\nu}\right)\hat{\boldsymbol{\theta}} \,, \tag{12}$$

where $\boldsymbol{K} = \boldsymbol{K}^{\mathrm{T}} > 0$ is a controller gain, $\boldsymbol{e}$ is given in (10), $\hat{\boldsymbol{\theta}}$ is an estimate of the true parameter and disturbance vector $\boldsymbol{\theta}$, and $\boldsymbol{\phi}\left(\dot{\boldsymbol{\nu}}_d, \boldsymbol{\nu}\right)$ is a matrix of known signals, and the update law

$$\dot{\hat{\boldsymbol{\theta}}} = -\boldsymbol{\Gamma}\phi^{\mathrm{T}}\left(\dot{\boldsymbol{\nu}}_d, \boldsymbol{\nu}\right)\boldsymbol{e} \tag{13}$$

with arbitrary initial conditions $\hat{\boldsymbol{\theta}}(0) = \hat{\boldsymbol{\theta}}_0 \in \mathbb{R}^8$, where $\boldsymbol{\Gamma} = \boldsymbol{\Gamma}^{\mathrm{T}} \in \mathbb{R}^{8\times 8}$, renders the origin of the error systems in (10) and $\tilde{\boldsymbol{\theta}} = \hat{\boldsymbol{\theta}} - \boldsymbol{\theta}$ stable with the error state $\boldsymbol{e}$ converging to zero for all initial values.

Proof: Consider the Lyapunov function candidate

$$V_1(\boldsymbol{e}, t) = \frac{1}{2}\boldsymbol{e}^{\mathrm{T}}\boldsymbol{M}\boldsymbol{e} \,, \tag{14}$$

which has time derivative along its trajectories

$$\begin{aligned} \dot{V}_1(\boldsymbol{e}, t) &= \boldsymbol{e}^{\mathrm{T}}\boldsymbol{M}\dot{\boldsymbol{e}} \\ &= \boldsymbol{e}^{\mathrm{T}}\left(-\boldsymbol{M}\dot{\boldsymbol{\nu}}_{\boldsymbol{d}} - \boldsymbol{D}_l\boldsymbol{\nu} - \boldsymbol{D}_n(\boldsymbol{\nu})\boldsymbol{\nu} + \boldsymbol{R}^{\mathrm{T}}(\psi)\boldsymbol{\tau}_c + \boldsymbol{\tau}\right), \end{aligned} \tag{15}$$

where (11) has been applied.

The term in the parenthesis of (15) (excluding $\boldsymbol{\tau}$) can be represented using a linear parameterized form, i.e.,

$$\boldsymbol{M}\dot{\boldsymbol{\nu}}_d + \boldsymbol{D}_l\boldsymbol{\nu} + \boldsymbol{D}_n(\boldsymbol{\nu})\boldsymbol{\nu} - \boldsymbol{R}^{\mathrm{T}}(\psi)\boldsymbol{\tau}_c = \boldsymbol{\phi}\left(\dot{\boldsymbol{\nu}}_d, \boldsymbol{\nu}\right)\boldsymbol{\theta} \,, \tag{16}$$

where $\boldsymbol{\phi}\left(\dot{\boldsymbol{\nu}}_d, \boldsymbol{\nu}\right) \in \mathbb{R}^{2\times 8}$ is a matrix of known, i.e., measured or generated, signals.

$$\boldsymbol{\phi}\left(\dot{\boldsymbol{\nu}}_d, \boldsymbol{\nu}\right) = \tag{17}$$
$$\begin{bmatrix} \dot{u}_d & 0 & u & 0 & |u|u & 0 & -\cos(\psi) & -\sin(\psi) \\ 0 & \dot{v}_d & 0 & v & 0 & |v|v & \sin(\psi) & -\cos(\psi) \end{bmatrix}$$

and $\boldsymbol{\theta} \in \mathbb{R}^8$ is a vector of unknown system parameters and external disturbances, i.e.,

$$\begin{aligned} \boldsymbol{\theta} = [&m - X_{\dot{u}},\, m - Y_{\dot{v}},\, -X_u,\, -Y_v, \\ &-X_{|u|u},\, -Y_{|v|v},\, \tau_c^N,\, \tau_c^E]^{\mathrm{T}} \,. \end{aligned} \tag{18}$$

Inserting the linear parameterized form of (16) into (15) gives

$$\dot{V}_1(\boldsymbol{e},t) = \boldsymbol{e}^{\mathrm{T}}\left(\boldsymbol{\tau} - \boldsymbol{\phi}\left(\dot{\boldsymbol{\nu}}_d, \boldsymbol{\nu}\right)\boldsymbol{\theta}\right) . \tag{19}$$

Inserting (12) into (19) gives

$$\dot{V}_1(\boldsymbol{e},t) = -\boldsymbol{e}^{\mathrm{T}}\boldsymbol{K}\boldsymbol{e} + \boldsymbol{e}^{\mathrm{T}}\boldsymbol{\phi}\left(\dot{\boldsymbol{\nu}}_d, \boldsymbol{\nu}\right)\tilde{\boldsymbol{\theta}} , \tag{20}$$

where $\tilde{\boldsymbol{\theta}} = \hat{\boldsymbol{\theta}} - \boldsymbol{\theta}$.

Next, define a second Lyapunov function candidate

$$V_2(\boldsymbol{e}, \tilde{\boldsymbol{\theta}}, t) = V_1(\boldsymbol{e}, t) + \frac{1}{2}\tilde{\boldsymbol{\theta}}^{\mathrm{T}}\boldsymbol{\Gamma}^{-1}\tilde{\boldsymbol{\theta}}. \tag{21}$$

Using Assumption 5 implies that $\dot{\tilde{\boldsymbol{\theta}}} = \dot{\hat{\boldsymbol{\theta}}}$, the time derivative of (21) along its trajectories is

$$\begin{aligned}\dot{V}_2(\boldsymbol{e}, \tilde{\boldsymbol{\theta}}, t) &= -\boldsymbol{e}^{\mathrm{T}}\boldsymbol{K}\boldsymbol{e} + \boldsymbol{e}^{\mathrm{T}}\boldsymbol{\phi}\left(\dot{\boldsymbol{\nu}}_d, \boldsymbol{\nu}\right)\tilde{\boldsymbol{\theta}} + \tilde{\boldsymbol{\theta}}^{\mathrm{T}}\boldsymbol{\Gamma}^{-1}\dot{\tilde{\boldsymbol{\theta}}} \\ &= -\boldsymbol{e}^{\mathrm{T}}\boldsymbol{K}\boldsymbol{e} + \tilde{\boldsymbol{\theta}}^{\mathrm{T}}\left(\boldsymbol{\phi}^{\mathrm{T}}\left(\dot{\boldsymbol{\nu}}_d, \boldsymbol{\nu}\right)\boldsymbol{e} + \boldsymbol{\Gamma}^{-1}\dot{\hat{\boldsymbol{\theta}}}\right) ,\end{aligned} \tag{22}$$

where (20) has been applied. Inserting the update law from (13) into (22) gives

$$\dot{V}_2(\boldsymbol{e}, \tilde{\boldsymbol{\theta}}, t) = -\boldsymbol{e}^{\mathrm{T}}\boldsymbol{K}\boldsymbol{e}, \leq 0 \,\forall\, \boldsymbol{e} . \tag{23}$$

This implies that $V_2(\boldsymbol{e}, \tilde{\boldsymbol{\theta}}, t) \leq V_2(\boldsymbol{e}, \tilde{\boldsymbol{\theta}}, 0)$ and that the origin of (21) is stable [20, Th. 4.1]. The time derivative of (23) is

$$\ddot{V}_2(\boldsymbol{e}, \tilde{\boldsymbol{\theta}}, t) = -2\boldsymbol{e}^{\mathrm{T}}\boldsymbol{K}\dot{\boldsymbol{e}} . \tag{24}$$

Assuming bounded initial conditions of $\boldsymbol{e}$ ensures that (24) is bounded. As such, (23) is uniformly continuous and hence convergence of (23) to zero is ensured through Barbălat's lemma, as in [21], [22], which in turn implies that $\boldsymbol{e} \to 0$ as $t \to \infty$. Combining the proof of stability with that of convergence ensures asymptotic stability in the sense of Lyapunov for the error state $\boldsymbol{e}$. ■

Remark 6: Theorem 1 does not guarantee convergence of $\tilde{\boldsymbol{\theta}}$ to zero. This would require the system to be persistently exciting [19, Ch. 4.2].

IV. Results

A. Net following and guidance law

The scenario considered for demonstration of the speed controllers is that of net-following, and as such the net-following algorithm and guidance law of [9] were used to provide reference speeds to the proposed controllers.

The control objective is to make the ROV follow a path $\mathcal{P} \in \mathcal{C}^2$ with a desired constant speed $U_d > 0$ and with the heading angle converging to some desired heading angle ψ_d(t).

The net-following algorithm is approximating the net structure as a plane based on the measured length of the beams from the DVL sensor. The normal vector of this plane is used when calculating the reference for the ROVs heading angle, $\psi_d(t)$, in order to point the ROV directly toward the net structure approximation. Further, the distance from the ROVs center of origin to the plane approximating the net structure, $d_{\text{net}}(t)$, is given by the inner product between the unit normal vector to the plane, and any vector from the ROV to the plane.

A LOS guidance law is used to calculate a course angle for the ROV, i.e.,

$$\chi_{\text{LOS}}(t) \triangleq \gamma_p(t) - \arctan\left(\frac{y_e(t)}{\Delta}\right) , \tag{25}$$

where $\chi_{\text{LOS}}(t)$ is the desired course angle, $\gamma_p(t)$ is the path-tangential angle, $y_e(t) = d_{\text{net}}(t) - d_d$ is the cross-track error with d_d as the desired distance to the net and $\Delta > 0$ is the lookahead distance [16]. The guidance law takes as inputs the ROV heading, $\psi(t)$, the path-tangential angle, $\gamma_p(t)$, and the cross-track error $y_e(t)$, and outputs the reference surge and sway speeds as follows:

$$u_r(t) \triangleq U_d \cos\left(-\psi(t) + \chi_{\text{LOS}}(t)\right) \tag{26}$$

$$v_r(t) \triangleq U_d \sin\left(-\psi(t) + \chi_{\text{LOS}}(t)\right) . \tag{27}$$

If the reference surge and sway speeds converge to their desired values, i.e.,

$$\lim_{t\to\infty} u(t) - u_r(t) = 0 \tag{28}$$

$$\lim_{t\to\infty} v(t) - v_r(t) = 0, \tag{29}$$

the guidance law (27) will ensure that the path $\mathcal{P}$ is followed with desired absolute speed $U_d \triangleq \sqrt{u_r^2 + v_r^2}$, i.e.,

$$\lim_{t\to\infty} y_e(t) = 0 \tag{30}$$

$$\lim_{t\to\infty} U(t) - U_d = 0. \tag{31}$$

See [9] for a full description of the net-following algorithm and stability analysis of the guidance law.

B. Simulation results

The derived controller (12) and update law (13) were implemented in FhSim [23], [24], a software platform and framework for mathematical modelling and numerical simulation with a focus on marine applications. The control plant model from (1) was used in the simulation to validate the controller. A model of an aquaculture net pen [25] was used to provide the ROV with an environment in which to move.

The ROV model from (1) and (2) was used in the simulation with the following parameters

$$\begin{aligned}\boldsymbol{M} &= \begin{bmatrix} m - X_{\dot{u}} & 0 \\ 0 & m - Y_{\dot{v}} \end{bmatrix} \\ &= \begin{bmatrix} 90 + 54 & 0 \\ 0 & 90 + 72 \end{bmatrix} = \begin{bmatrix} 144 & 0 \\ 0 & 162 \end{bmatrix}\end{aligned} \tag{32}$$

$$\boldsymbol{D}_l = \begin{bmatrix} 250 & 0 \\ 0 & 200 \end{bmatrix} \tag{33}$$

$$\boldsymbol{D}_n = \begin{bmatrix} 350 & 0 \\ 0 & 350 \end{bmatrix} . \tag{34}$$

The current and 1st order wave forces were given by $\tau_c = \begin{bmatrix} 20 & 20 \end{bmatrix}^{\mathrm{T}}$. The parameters of the controllers used in the simulation are listed in Table I.

TABLE I: Controller parameters used in the simulations.

Parameter	Value
$\boldsymbol{K}$	diag $(500, 500)$
$\boldsymbol{\Gamma}$	$350\ \mathbb{I}^{8\times 8}$
ζ_u, ζ_v	1
ω_u, ω_v	2
Δ	1

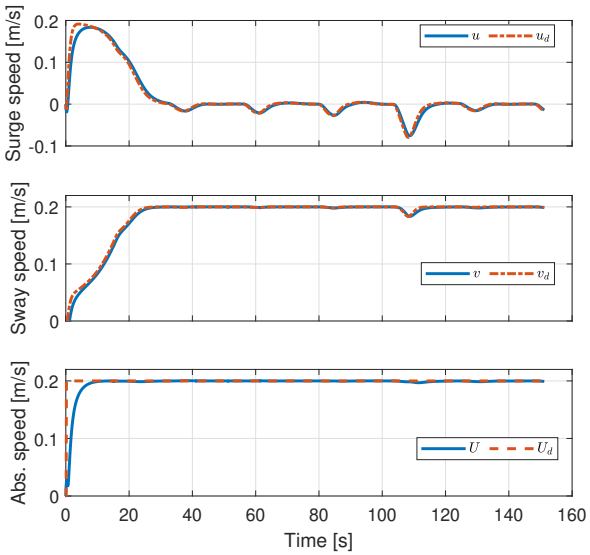

Fig. 1: Simulation results showing the tracking of the desired surge and sway speeds, as well as the absolute speed.

The ROV was commanded to follow the net structure with desired speed $U_d = 0.2$ m/s and desired distance from the net of $d_d = 2$ m. The ROV was initially placed 5 meters from the net structure, at 5 meters depth, with a heading angle of $\psi = \pi$. All estimated parameters, and the reference models, were initialized at zero.

From Figure 1, we see that the desired surge and sway speeds, as well as the desired absolute speed are accurately tracked by the controller. Figure 2 shows that the desired distance to the net is maintained after an initial period of convergence of about 20 seconds. Further, Figure 2 shows that the desired heading and depth are accurately tracked by the adaptive backstepping controller from [15].

Figures 3 and 4 show the estimated parameters in the surge and sway degrees of freedom, respectively. These do not converge to the actual values, but this is not required for $\boldsymbol{e}$ to converge to zero according to Theorem 1.

C. Experimental results

The controller was validated in a field trial performed at the SINTEF ACE full-scale laboratory for aquaculture technologies [26], see Figure 5. The ROV used is an Argus Mini [27], a 90 kg Observation-class ROV which has 4 thrusters in the horizontal plane and 2 thrusters in the vertical plane. The ROV is slightly positively buoyant and passively stabilized in the roll and pitch degrees of freedom. The ROV is controlled through an in-house graphical user interface (GUI) which allows the operator to manually control the

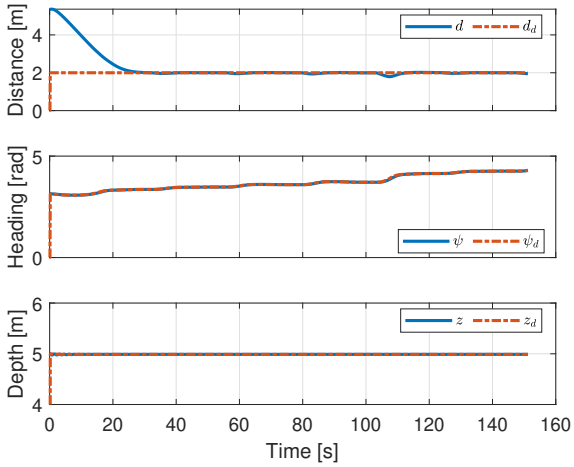

Fig. 2: Simulation results showing the tracking of the desired distance to the net, the heading angle and the depth.

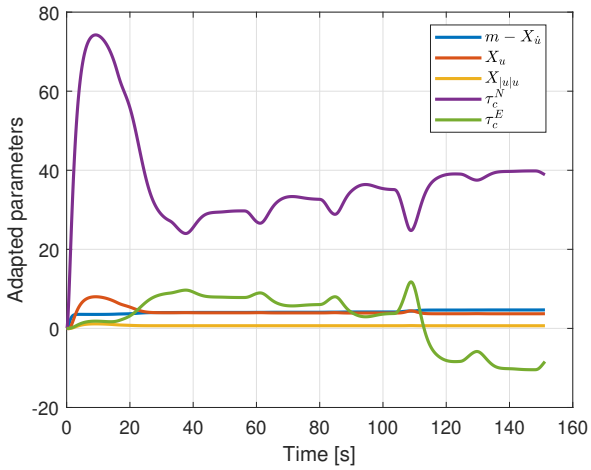

Fig. 3: The estimated parameters in the surge direction during the simulation.

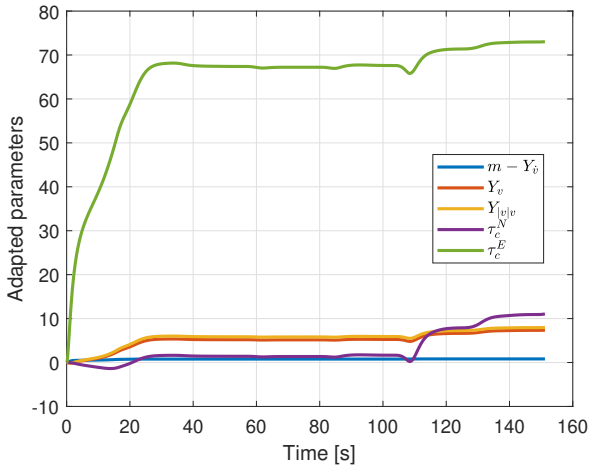

Fig. 4: The estimated parameters in the sway direction during the simulation.

Fig. 5: SINTEF ACE full-scale laboratory for aquaculture technologies. Photo: Magnus O. Pedersen.

TABLE II: Controller parameters used in the field trial

Parameter	Value
$\boldsymbol{K}$	diag $(300, 300)$
$\boldsymbol{\Gamma}$	$150\ \mathbb{I}^{8\times 8}$
ζ_u, ζ_v	1
ω_u, ω_v	1
Δ	1
$k_{p,u}$, $k_{p,v}$	200
$k_{i,u}$, $k_{i,v}$	5

ROV and activate functions such as net-following and dynamic positioning.

The speed controller alongside the net-following algorithm, guidance law, and an extended Kalman filter (EKF) for the Argus Mini ROV based on [28], are running in FhSim. The GUI is communicating with the FhSim framework through the Inter-Module Communication (IMC) protocol [29]. Commands are sent to the ROV through a serial connection. The ROV is equipped with a depth sensor, magnetic compass, and a forward-facing Nortek 1000 DVL for measuring the distance, heading, and velocity relative to the net. The EKF provides filtered estimates of the controlled states, i.e., u, v, ψ, and the depth, D. The speed controller from (12) with update law (13) is used. The heading angle and depth are controlled using the adaptive backstepping controller from [15]. The parameters used in the field trial are listed in Table II. A block diagram is shown in Figure 6.

The ROV was lowered into the net pen and manually operated to the starting location which was approximately 3 meters from the net. The ROV was facing the net prior to the activation of the net-following algorithm to ensure that the forward-facing DVL made contact with the net structure. The ROV was commanded to maintain a distance of 2.5 meters to the net, a depth of 5 meters and to have a velocity of $U_d = 0.2$ m/s. The vehicle was commanded to travel in the starboard direction between $t \sim 30$ and $t \sim 100$, and in the port direction between $t \sim 100$ and $t \sim 180$.

The net pen used in the experiments contains approximately 200.000 living Atlantic salmon (*Salmo Salar*). The fish often swim in front of the ROV and disrupt the beams from the DVL, resulting in signal loss [30]. The control system is designed to stop the net-following procedure if the DVL signal is lost, and continue when the signal returns (yellow line and right-side y-axis of Figures 8 and 7). The ocean current during the trial was measured to be 0.09 m/s with a direction of 39° at a depth of 4.5 meters. This measurement was taken from a buoy located outside the net pen in which the experiment was carried out.

Figure 7 shows the results of speed tracking from one of the experiments. The ROV operated manually for the first ~ 30 seconds before the net-following algorithms and the speed controllers were turned on. The top plot of Figure 7 shows the surge speed u, the middle plot shows the sway speed v, and the bottom plot shows the absolute speed U. From Figure 7, it is clear that the controller brings the surge and sway speeds to their desired values. The DVL experienced signal loss between $t \sim 80$ to $t \sim 90$ seconds which turns off the algorithm, hence the desired speeds are not tracked in that time period. Figure 8 shows estimates of the ROVs distance and heading relative to the net, and its depth. The desired distance to the net is maintained with small deviations. Some measurement noise is experienced between $t \sim 160$ to $t \sim 170$ which may be caused by fish disrupting the DVL signals.

Figure 8 also shows the heading angle and the depth, controlled using a controller similar to the adaptive backstepping controller from [15] with parameters tuned for this experiment. The desired depth is accurately tracked, while the heading experiences some deviation between $t \sim 60$ and $t \sim 75$ seconds. From the top two plots of Figure 7 it can be seen that the surge and sway speeds also suffer from inaccuracies during this time period and the coupling between the degrees of freedom is most likely causing this deviation in heading. The heading is more accurately tracked between $t \sim 90$ to $t \sim 160$.

Figures 9 and 10 show the estimated parameters during the field trial in the surge and sway degree of freedom, respectively. Note that the adaptation stops when the DVL signal is lost. When the DVL signal returns the adaptation is re-started, but it is also re-initialized at zero. This is purposefully implemented to avoid sudden jumps and kinks in the control input when the DVL locks to the net again.

In the interest of comparison, PI speed controllers were also tested during the field trial. These controllers were tuned based on operator experience combined with a trial-and-error approach. Controller parameters are listed in Table II. During the tuning, it was found that the integral parts of the controllers were influenced by the presence of measurement noise and thus had to be chosen with great care. This resulted in conservative values for the integral parts. This is in line with findings reported in [31]. Figure 11 shows the results. A deviation is clearly present in the sway degree of freedom which is probably caused by the conservative choice of integral gain. This deviation again leads to a deviation in the desired absolute speed. Note that these deviations are not present when using the proposed controller.

V. Conclusion and Future Work

An adaptive speed controller for the surge and sway speeds of an ROV has been presented in this paper. It is shown through Lyapunov analysis that the state error variable and the estimated parameters are stable and that the state error converges to zero asymptotically. The developed controllers were demonstrated using a net-following algorithm and a

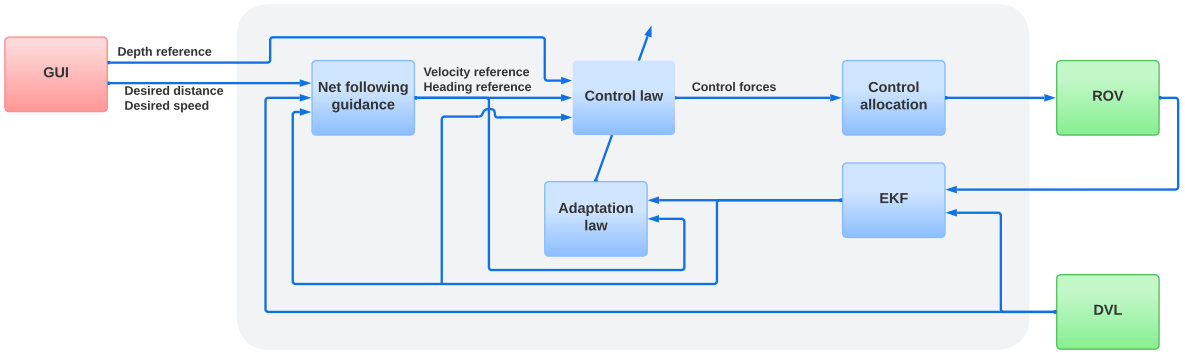

Fig. 6: Block diagram of the guidance, navigation, and control system used in the field trials. The area marked in grey were programmed in FhSim on the topside computer.

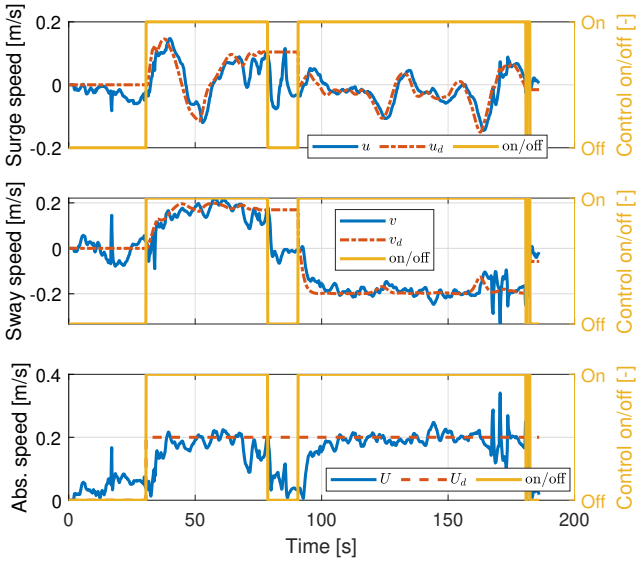

Fig. 7: Experimental trial showing tracking of surge, sway and absolute speed, respectively, using the proposed controller.

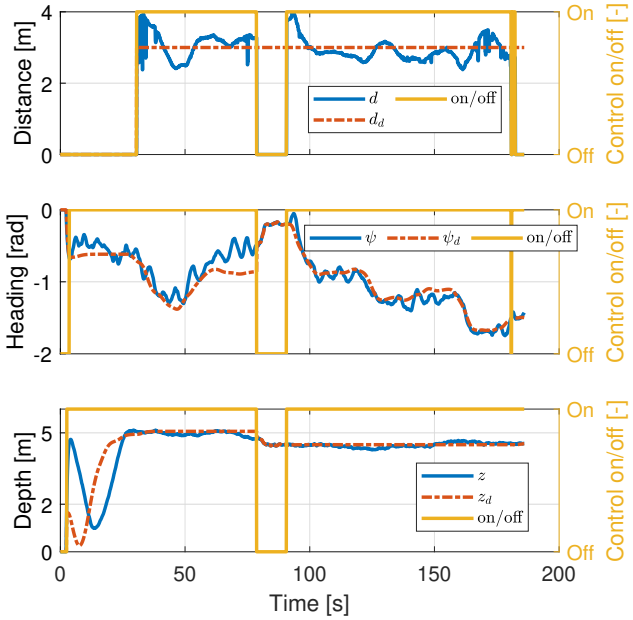

Fig. 8: Experimental trial showing tracking of distance to net, heading angle and depth, respectively, using the proposed controller. The DVL signal was lost between $t = 75$s and $t = 90$s.

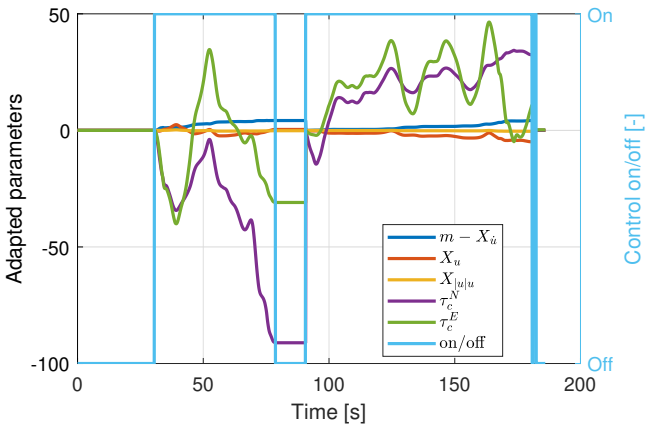

Fig. 9: Estimated parameters in the surge direction during the field trial.

guidance law developed for ROV operations in aquaculture net pens. The presented controllers were validated in both simulations and field trials at a full-scale fish farm. Future work may involve extending the proposed controller to also include the heave speed, and to investigate the parameter estimation capabilities of the proposed controller.

Acknowledgement

The research was conducted at SINTEF Ocean's full-scale aquaculture facility ACE with support from the ACE team. The authors received internal funding and support from SINTEF Ocean. The work is partly supported by the Norwegian Research council projects CHANGE (grant no. 313737), SFI Exposed (grant no. 237790) and Artifex (grant no. 256241).

References

[1] M. Føre, K. Frank, T. Norton, E. Svendsen, J. A. Alfredsen, T. Dempster, H. Eguiraun, W. Watson, A. Stahl, L. M. Sunde, et al., Precision fish farming: A new framework to improve production in aquaculture, biosystems engineering 173 (2018) 176–193.

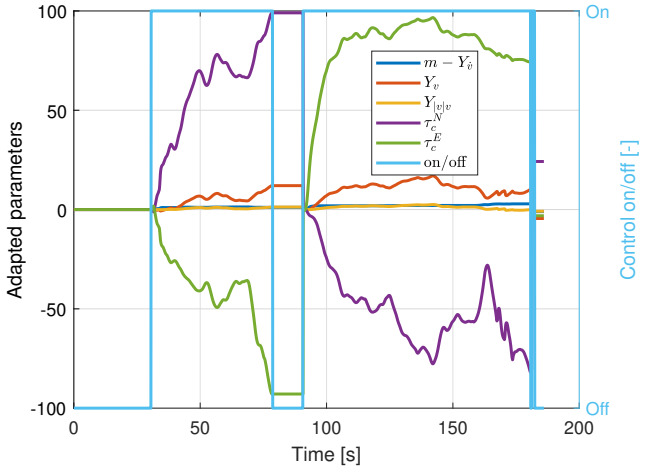

Fig. 10: Estimated parameters in the sway direction during the field trial.

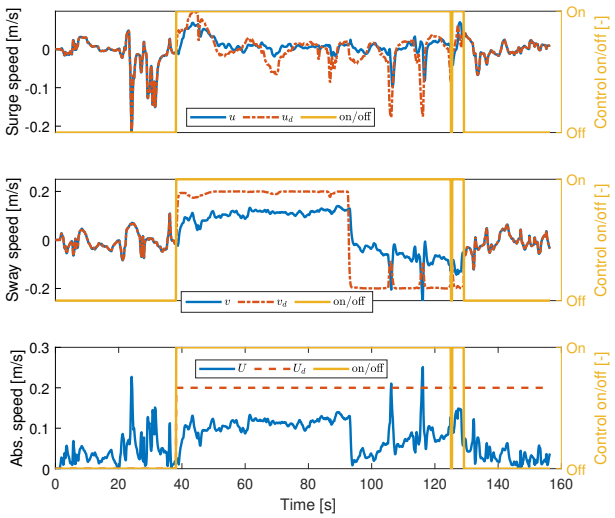

Fig. 11: Experimental trial showing tracking of surge, sway and absolute speed, respectively, using a PI controller.

[2] H. M. Føre, T. Thorvaldsen, Causal analysis of escape of Atlantic salmon and rainbow trout from Norwegian fish farms during 2010–2018, Aquaculture 532 (2021) 736002.

[3] G. H. Bolstad, K. Hindar, G. Robertsen, B. Jonsson, H. Sægrov, O. H. Diserud, P. Fiske, A. J. Jensen, K. Urdal, T. F. Næsje, et al., Gene flow from domesticated escapes alters the life history of wild atlantic salmon, Nature Ecology & Evolution 1 (5) (2017) 1–5.

[4] T. Forseth, B. T. Barlaup, B. Finstad, P. Fiske, H. Gjøsæter, M. Falkegård, A. Hindar, T. A. Mo, A. H. Rikardsen, E. B. Thorstad, et al., The major threats to Atlantic salmon in Norway, ICES Journal of Marine Science 74 (6) (2017) 1496–1513.

[5] Regulation on the operation of aquaculture facilities, Norwegian Ministry of Trade, Industry and Fisheries (2022-08-24).
URL https://lovdata.no/dokument/SF/forskrift/2008-06-17-822#KAPITTEL_3

[6] A. J. L. Solem, Analysis of current ROV operations in the Norwegian aquaculture-reducing risk in exposed aquaculture operations, Master's thesis, NTNU (2017).

[7] Norwegian Directorate of Fisheries, Website, https://www.fiskeridir.no/Akvakultur/erfaringsbase-romming/erfaringshendelser/notinspeksjon-med-rov-fleire-tilfelle-der-skadane-pa-nota-ikkje-vart-oppdaga, acessed 07.12.2022 (2022).

[8] H. Bjelland, M. Føre, P. Lader, D. Kristiansen, I. Holmen, A. Fredheim, E. Grøtli, D. Fathi, F. Oppedal, I. Utne, et al., Exposed aquaculture in Norway: Technologies for robust operation in rough conditions, in: Proc. of MTS/IEEE OCEANS'15, 2015.

[9] H. B. Amundsen, W. Caharija, K. Y. Pettersen, Autonomous ROV inspections of aquaculture net pens using DVL, IEEE Journal of Oceanic Engineering 47 (1) (2021) 1–19.

[10] T. I. Fossen, M. Breivik, R. Skjetne, Line-of-sight path following of underactuated marine craft, Proceedings of the 6th IFAC MCMC, Girona, Spain (2003) 244–249.

[11] H. Ø. Karlsen, H. B. Amundsen, W. Caharija, M. Ludvigsen, Autonomous aquaculture: Implementation of an autonomous mission control system for unmanned underwater vehicle operations, in: OCEANS 2021: San Diego–Porto, IEEE, 2021, pp. 1–10.

[12] M. Bjerkeng, T. Kirkhus, W. Caharija, J. T. Thielemann, H. B. Amundsen, S. Johan Ohrem, E. Ingar Grøtli, ROV navigation in a fish cage with laser-camera triangulation, Journal of Marine Science and Engineering 9 (1) (2021) 79.

[13] S. Soylu, A. A. Proctor, R. P. Podhorodeski, C. Bradley, B. J. Buckham, Precise trajectory control for an inspection class ROV, Ocean Engineering 111 (2016) 508–523.

[14] D. d. A. Fernandes, A. J. Sørensen, K. Y. Pettersen, D. C. Donha, Output feedback motion control system for observation class ROVs based on a high-gain state observer: Theoretical and experimental results, Control Engineering Practice 39 (2015) 90–102.

[15] S. J. Ohrem, H. B. Amundsen, W. Caharija, C. Holden, Robust adaptive backstepping DP control of ROVs, Control Engineering Practice 127 (2022) 105282.

[16] T. I. Fossen, Handbook of marine craft hydrodynamics and motion control, John Wiley & Sons, 2011.

[17] G. Antonelli, Underwater robots, Springer, 2014.

[18] K. E. Jónsdóttir, P. Klebert, Z. Volent, J. A. Alfredsen, Characteristic current flow through a stocked conical sea-cage with permeable lice shielding skirt, Ocean Engineering 223 (2021) 108639.

[19] P. A. Ioannou, J. Sun, Robust adaptive control, Courier Dover Publications, 2012.

[20] H. K. Khalil, Nonlinear systems, Vol. 3, Prentice Hall, 2002.

[21] S. J. Ohrem, T. T. Kristoffersen, C. Holden, Adaptive feedback linearizing control of a gas liquid cylindrical cyclone, in: 2017 IEEE Conference on Control Technology and Applications (CCTA), IEEE, 2017, pp. 1981–1987.

[22] T. I. Fossen, M. Paulsen, Adaptive feedback linearization applied to steering of ships (1993).

[23] K.-J. Reite, M. Føre, K. G. Aarsæther, J. Jensen, P. Rundtop, L. T. Kyllingstad, P. C. Endresen, D. Kristiansen, V. Johansen, A. Fredheim, FhSim—time domain simulation of marine systems, in: International Conference on Offshore Mechanics and Arctic Engineering, Vol. 45509, American Society of Mechanical Engineers, 2014, p. V08AT06A014.

[24] B. Su, K.-J. Reite, M. Føre, K. G. Aarsæther, M. O. Alver, P. C. Endresen, D. Kristiansen, J. Haugen, W. Caharija, A. Tsarau, A multipurpose framework for modelling and simulation of marine aquaculture systems, in: International Conference on Offshore Mechanics and Arctic Engineering, Vol. 58837, American Society of Mechanical Engineers, 2019, p. V006T05A002.

[25] B. Su, E. Kelasidi, K. Frank, J. Haugen, M. Føre, M. O. Pedersen, An integrated approach for monitoring structural deformation of aquaculture net cages, Ocean Engineering 219 (2021) 108424.

[26] SINTEF Ocean, Website, https://www.sintef.no/en/all-laboratories/ace/, acessed 22.11.2022 (2022).

[27] Argus Remote Systems, Website, https://www.argus-rs.no/argus-rovs/11/argus-mini, acessed 22.11.2022 (2022).

[28] M. Candeloro, A. J. Sørensen, S. Longhi, F. Dukan, Observers for dynamic positioning of ROVs with experimental results, IFAC Proceedings Volumes 45 (27) (2012) 85 – 90, 9th IFAC Conference on Manoeuvring and Control of Marine Craft.

[29] R. Martins, P. S. Dias, E. R. Marques, J. Pinto, J. B. Sousa, F. L. Pereira, Imc: A communication protocol for networked vehicles and sensors, in: Oceans 2009-Europe, IEEE, 2009, pp. 1–6.

[30] P. Rundtop, K. Frank, Experimental evaluation of hydroacoustic instruments for ROV navigation along aquaculture net pens, Aquacultural Engineering 74 (2016) 143–156.

[31] R. Skjetne, T. I. Fossen, On integral control in backstepping: Analysis of different techniques, in: Proceedings of the 2004 American control conference, Vol. 2, IEEE, 2004, pp. 1899–1904.